Inhibitory proteins block substrate access to the membrane-embedded active site of *Bacillus subtilis* intramembrane protease SpoIVFB

Sandra Olenic[a], Lim Heo[a], Michael Feig[a], and Lee Kroos[a,1]

[a]Department of Biochemistry and Molecular Biology, Michigan State University, East Lansing, MI 48824

[1]To whom correspondence should be addressed. Email: kroos@msu.edu

Abstract

Intramembrane proteases function in numerous signaling pathways that impact health, but how their membrane-embedded active sites interact with modulators is poorly understood. We examined inhibition of intramembrane metalloprotease SpoIVFB by proteins BofA and SpoIVFA. We found that BofA residues in and near a predicted transmembrane segment are required for SpoIVFB inhibition, and cross-linking experiments indicated that this transmembrane segment occupies the SpoIVFB active site region. BofA and SpoIVFA neither prevented SpoIVFB from interacting with substrate in co-purification assays nor interfered with cross-linking between the C-terminal regions of substrate and SpoIVFB. However, the inhibitory proteins did interfere with cross-linking between the SpoIVFB active site region and the substrate N-terminal Proregion, which is normally cleaved. We conclude that BofA and SpoIVFA block substrate access to the membrane-embedded active site of SpoIVFB. A structural model was built of SpoIVFB in complex with BofA and parts of SpoIVFA and substrate, using partial homology and constraints from cross-linking and co-evolutionary analyses. The model predicts that conserved BofA residues interact to stabilize a transmembrane segment and a membrane-embedded C-terminal region. SpoIVFA is predicted to bridge the BofA C-terminal region and SpoIVFB, forming a membrane-embedded inhibitory complex. Implications for design of intramembrane metalloprotease inhibitors are discussed.

Introduction

Intramembrane proteases (IPs) are membrane proteins containing a membrane-embedded active site. IPs cleave membrane-associated substrates within a transmembrane segment (TMS) or near the membrane surface in a process referred to as regulated intramembrane proteolysis (RIP) (1). Released substrate fragments impact diverse signaling pathways in a wide variety of organisms (2). There are four known IP families: intramembrane metalloproteases (IMMPs) like SpoIVFB, aspartyl proteases like presenilins, serine proteases (rhomboids), and the glutamyl protease Rce1 (2, 3). Crystal structures have been solved for one or more IP in each family (3-8), revealing that TMSs arrange to form a channel that delivers water to the active site for hydrolysis of a substrate peptide bond. Structures have also been solved for rhomboid·peptide inhibitor complexes (9, 10) and for γ-secretase·substrate complexes (11, 12), which may guide the design of IP modulators as therapeutics or for other purposes.

IMMPs activate transcription factors via RIP in all three domains of life (1, 2). In humans, S2P is involved in regulation of cholesterol homeostasis and responses to endoplasmic reticulum stress and viral infection (13, 14). S2P homologs in plants and in the pathogenic fungus *Cryptococcus neoformans* play important roles in chloroplast development and virulence, respectively (15, 16). In bacteria, IMMPs enhance pathogenicity, control stress responses and polar morphogenesis, produce mating signals, and clear signal peptides from the membrane (17-19). In *Bacillus* and *Clostridium* species, SpoIVFB cleaves inactive Pro-σ^K to σ^K, which directs RNA polymerase to transcribe genes necessary for endospore formation (18, 20). Endospores are dormant and are able to survive harsh environmental conditions (21), enhancing the persistence of pathogenic species (22, 23). Knowledge of SpoIVFB interactions with its

inhibitory proteins, BofA and SpoIVFA (24-26), could lead to new strategies to manipulate endosporulation and other processes involving IMMPs in bacteria and eukaryotes.

During endospore formation, *B. subtilis* forms a polar septum that divides the mother cell (MC) and forespore (FS) compartments (27) (Fig. S1). The MC engulfs the FS, surrounding it with a second membrane and pinching it off within the MC. SpoIVFB, BofA, and SpoIVFA form a complex in the outer FS membrane during engulfment (28-30). BofA was implicated as the direct inhibitor of SpoIVFB (31), while SpoIVFA appeared to localize and stabilize the heterotrimer (30, 32). Signaling from the FS relieves inhibition of SpoIVFB (Fig. S1). Two proteases, SpoIVB and CtpB, are exported into the space between the two membranes surrounding the FS (33, 34). SpoIVB cleaves the C-terminal end of SpoIVFA (35-38) and CtpB can cleave the C-terminal ends of both SpoIVFA and BofA (36, 37, 39). Once inhibition is removed, SpoIVFB cleaves the N-terminal 21-residue Proregion from Pro-σ^K, releasing σ^K into the MC (40-42). σ^K directs RNA polymerase to transcribe genes whose products form the spore coat and lyse the MC, releasing a mature spore (43, 44).

Cleavage of Pro-σ^K by SpoIVFB can be reproduced by expressing these proteins in *Escherichia coli* (31) (Fig. 1A). Cleavage could be inhibited by additionally producing GFPΔ27BofA (a functional fusion protein lacking predicted TMS1 of BofA) and SpoIVFA (31, 39). However, we found that the extent of cleavage inhibition was incomplete and variable. Here, we describe an improved cleavage inhibition assay. Using the assay and bioinformatics, we identified three conserved residues of BofA important for inhibition of SpoIVFB in *E. coli* and in sporulating *B. subtilis.* One of the residues, N48, is near the middle of BofA TMS2, close to the sole Cys residue of BofA, C46. We exploited C46 for disulfide cross-linking experiments that showed TMS2 of BofA can occupy the SpoIVFB active site region. These experiments

relied on single-Cys variants of SpoIVFB created previously and used to cross-link residues predicted to be near the active site with residues near the cleavage site in single-Cys variants of Pro-σ^K (45). We created additional single-Cys variants of SpoIVFB, Pro-σ^K, and BofA, as well as functional Cys-less SpoIVFA, and performed disulfide cross-linking experiments. We found that BofA and SpoIVFA interfere with cross-linking between the N-terminal Proregion of Pro-σ^K and the SpoIVFB active site region, indicating that the inhibitory proteins block substrate access to the IMMP active site. The results were used in combination with prior cross-linking studies (45, 46), partial homology, and evolutionary co-variation of amino acid residues, to constrain a structural model of SpoIVFB in complex with BofA and parts of SpoIVFA and Pro-σ^K. The model predicts that conserved residues in TMS2 and the C-terminal region of BofA interact, and that SpoIVFA bridges the BofA C-terminal region and SpoIVFB to form a membrane-embedded inhibitory complex.

Results

BofA and SpoIVFA Can Prevent Cleavage of Pro-σ^K by SpoIVFB in *E. coli*. To study RIP of Pro-σ^K, *E. coli* was engineered to synthesize variants of SpoIVFB and Pro-σ^K, and the two inhibitory proteins, BofA and SpoIVFA, in various combinations. The SpoIVFB variant cytTM-SpoIVFB-$FLAG_2$-His_6 (cytTM-SpoIVFB) (Fig. 1A) contains cytTM (47), which improves accumulation (42). The substrate variant Pro-σ^K(1-127)-His_6 [Pro-σ^K(1-127)] lacks the C-terminal half of Pro-σ^K, but can be cleaved by SpoIVFB and the cleavage product can easily be separated from Pro-σ^K(1-127) by SDS-PAGE (48) [Note: Pro-σ^K(1-126) was renamed Pro-σ^K(1-127) as explained in (46)]. When Pro-σ^K(1-127) was produced with cytTM-SpoIVFB, cleavage was abundant (Fig. 1B, lane 1), as shown previously (42). To quantify cleavage, we measured

the abundance of cleavage product and divided that by the amount of Pro-σ^K(1-127) plus cleavage product, which resulted in a cleavage ratio of 0.78 $\pm$ 0.02. The additional production of GFPΔ27BofA and SpoIVFA from a second plasmid reduced the cleavage ratio to 0.3 $\pm$ 0.08, but cleavage product was visible (lane 2). A similar result was seen when full-length BofA (for which no antibody has been described) and SpoIVFA were produced from a second plasmid (lane 3). Since the second plasmid had the same replication origin as the plasmid used to produce Pro-σ^K(1-127) and cytTM-SpoIVFB (i.e., the two plasmids were "incompatible"), the copy number of the two plasmids may be unequal in some cells, despite using different selection markers to try to maintain both plasmids. Unequal copy numbers could result in Pro-σ^K(1-127) cleavage in cells producing too little of the inhibitory proteins. Therefore, we designed single plasmids to synthesize all four proteins, which we called "pET Quartet plasmids." When pET Quartets produced either GFPΔ27BofA (lane 4) or BofA (lane 5), inhibition improved, resulting in very little Pro-σ^K(1-127) cleavage. A longer exposure of the immunoblot revealed a faint cleavage product with pET Quartet GFPΔ27BofA, but not with pET Quartet BofA, indicating that full-length BofA inhibits cleavage slightly better than GFPΔ27BofA.

We tested whether both GFPΔ27BofA and SpoIVFA are required for cleavage inhibition by engineering "pET Triplet plasmids" to synthesize Pro-σ^K(1-127), cytTM-SpoIVFB, and either GFPΔ27BofA or SpoIVFA. With pET Triplet GFPΔ27BofA, cleavage of Pro-σ^K(1-127) was observed (ratio = 0.7 $\pm$ 0.1), but accumulation of cytTM-SpoIVFB, Pro-σ^K(1-127), and cleavage product was greatly diminished (Fig. 1C, lane 2), suggesting that GFPΔ27BofA inhibits synthesis and/or enhances degradation of the other proteins when SpoIVFA is absent. With pET Triplet SpoIVFA (lane 3), the cleavage ratio (0.6 $\pm$ 0.05) and accumulation of cytTM-SpoIVB, Pro-σ^K(1-127), and cleavage product were similar to the control plasmid that synthesized only

cytTM-SpoIVFB and Pro-σ^K(1-127) (lane 1). We conclude that both GFPΔ27BofA and SpoIVFA are necessary to strongly inhibit Pro-σ^K(1-127) cleavage by cytTM-SpoIVB in *E. coli* (lane 4). Both inhibitory proteins are required to prevent cleavage of Pro-σ^K by SpoIVFB during *B. subtilis* sporulation (24, 30, 49).

Efficient relief of SpoIVFB inhibition by BofA and SpoIVFA during *B. subtilis* sporulation requires SpoIVB and CtpB (Fig. S1), but SpoIVB alone can partially relieve inhibition (34, 36, 37, 39). Likewise, SpoIVB partially relieved inhibition when produced in *E. coli* from "pET Quintet plasmids" (i.e., pET Quartet plus SpoIVB) (Supplemental Results and Fig. S2). In the absence of SpoIVB, an F66A substitution in SpoIVFB-YFP can partially overcome inhibition by BofA and SpoIVFA during *B. subtilis* sporulation (49). The F66A substitution in cytTM-SpoIVFB likewise partially overcame inhibition by GFPΔ27BofA and SpoIVFA when produced from pET Quartet in *E. coli* (Supplemental Results and Fig. S3). Hence, the heterologous system mimics the endogenous pathway of *B. subtilis* in these respects. We next exploited the improved cleavage inhibition assay based on pET Quartet plasmids in *E. coli* to identify residues of BofA important for SpoIVFB inhibition.

Three Conserved Residues of BofA Are Important for Inhibition of SpoIVFB in *E. coli*. To identify residues of BofA that may play a role in SpoIVFB inhibition, an alignment of 70 BofA orthologs was made (Fig. S4A). The majority of conserved residues reside in predicted TMS2 and the C-terminal region, which could explain why GFPΔ27BofA (lacking predicted TMS1) is a functional inhibitor (30, 31) (Fig. 1B). Most endospore formers encode BofA, but about half lack a recognizable gene for SpoIVFA (20, 50). A smaller alignment (Fig. S4B) was made to see if additional residues are conserved in BofA orthologs of species encoding SpoIVFA. In total,

142 17 residues of interest were conserved in BofA: 13 within TMS2 and the C-terminal region of
143 the larger alignment, and 4 from the C-terminal region of the smaller alignment.
144 We substituted conserved residues in GFPΔ27BofA with alanine to investigate their
145 roles. Since deletion of three residues from the C-terminal end of BofA caused a loss of function
146 or stability in *B. subtilis* (26, 51), we also made Ala substitutions for F85 and I87 (as well as I86,
147 which is conserved) in GFPΔ27BofA. Each GFPΔ27BofA variant was co-produced with Pro-
148 σ^K(1-127), cytTM-SpoIVFB, and SpoIVFA from pET Quartet plasmids in *E. coli*, and the Pro-
149 σ^K(1-127) cleavage ratio was quantified (Fig. 2). Three GFPΔ27BofA variants, N48A, N61A,
150 and T64A (lanes 4, 7 & 8), led to the greatest cleavage ratios, indicating that these substitutions
151 strongly impaired inhibition of cytTM-SpoIVFB. However, less of the N61A and T64A variants
152 accumulated than most of the other GFPΔ27BofA variants, and for all three variants, less
153 SpoIVFA and cytTM-SpoIVFB accumulated, indicating that the variants reduce the synthesis
154 and/or stability of proteins that normally form the SpoIVFB inhibition complex (24, 30, 31, 39,
155 49). We reasoned that accumulation of the proteins may differ in *E. coli* and sporulating *B.*
156 *subtilis*, so we examined the effects of GFPΔ27BofA N48A, N61A, and T64A variants during
157 sporulation (see below).
158 Importantly, deletion of three residues from the C-terminal end of GFPΔ27BofA strongly
159 impaired inhibition of cytTM-SpoIVFB in *E. coli* (Supplemental Results and Fig. S5A),
160 mimicking results obtained for the endogenous pathway of *B. subtilis* (26, 51). We also used
161 pET Quartet plasmids in *E. coli* to show that nine residues preceding predicted TMS2 of
162 GFPΔ27BofA contribute to its inhibitory function (Supplemental Results and Fig. S5B).
163

The Conserved Residues of BofA Are Important for SpoIVFB Inhibition during *B. subtilis* Sporulation. A *B. subtilis spoIVB165 bofA::erm* double mutant provides a genetic background to test the effects of Ala substitutions on BofA function during sporulation. The *spoIVB165* null mutation alone would block Pro-σ^K cleavage, but cleavage is restored in the *spoIVB165 bofA::erm* double mutant, and ectopic production of GFPΔ27BofA under control of an MC-specific promoter in the double mutant leads to inhibition of SpoIVFB (30, 31).

To test the effects of the three GFPΔ27BofA variants (N48A, N61A, and T64A) during sporulation, each was produced ectopically under control of the *bofA* promoter in the *spoIVB165 bofA::erm* double mutant background (Fig. 3A). As a control, in wild-type *B. subtilis* strain PY79, BofA and SpoIVFA inhibited Pro-σ^K cleavage until between 4 and 5 h poststarvation (PS), and the levels of SpoIVFA and SpoIVFB decreased between 4 and 5 h PS (lanes 1 & 2). For the *spoIVB165* single mutant, very little Pro-σ^K cleavage was observed, as expected, and the SpoIVFA and SpoIVFB levels did not decrease at 5 h (lanes 3 & 4). For the *spoIVB165 bofA::erm* double mutant, inhibition of SpoIVFB was expected to be lost, and in agreement the Pro-σ^K cleavage ratio at 4 h (lane 5) was greater than for the wild-type strain at 4 h (lane 1) and similar to the ratios at 5 h (lanes 2 and 6). Very little SpoIVFA and SpoIVFB was detected (lanes 5 & 6), consistent with the need for BofA to stabilize these proteins (30). As expected, ectopic production of GFPΔ27BofA in the double mutant inhibited SpoIVFB so that little Pro-σ^K cleavage was observed, and the SpoIVFA and SpoIVFB levels did not decrease at 5 h (lanes 7 & 8), similar to the *spoIVB165* single mutant (lanes 3 & 4). GFPΔ27BofA allowed a greater Pro-σ^K cleavage ratio at 5 h (lane 8) than BofA (lane 4), suggesting that full-length BofA is a slightly better inhibitor of SpoIVFB during *B. subtilis* sporulation, as observed in *E. coli* (Fig. 1B, longer exposure).

Strikingly, ectopic production of the GFPΔ27BofA N48A or N61A variant in the double mutant did not inhibit SpoIVFB, as Pro-σ^K was cleaved at 4 h (Fig. 3A, lanes 9 & 11). The level of the N48A variant (lanes 9 & 10) was comparable with GFPΔ27BofA (lanes 7 & 8), but less of the N61A variant was observed, especially at 5 h (lanes 11 & 12). In comparison with the strain that produced GFPΔ27BofA, the SpoIVFA level was normal in the strain that produced the N48A variant, but less SpoIVFB was observed, and less of both SpoIVFA and SpoIVFB was observed in the strain producing the N61A variant. Production of the T64A variant in the double mutant (lanes 13 & 14) showed a pattern similar to the wild-type strain (lanes 1 & 2); Pro-σ^K cleavage increased between 4 and 5 h, and the levels of SpoIVFA and SpoIVFB decreased. The levels of all three proteins were slightly lower in the strain producing the T64A variant than in the wild-type strain. The level of the T64A variant was similar to the N48A and N61A variants at 4 h, yet the Pro-σ^K cleavage ratio was lower (lanes 9, 11 & 13), suggesting that the T64A variant inhibits SpoIVFB, although not as well as GFPΔ27BofA (lane 7). We conclude that the three conserved residues of BofA are important for SpoIVFB inhibition during sporulation.

Since GFPΔ27BofA co-localizes with SpoIVFA and SpoIVFB to the outer FS membrane during sporulation (28-30), we examined the ability of the GFPΔ27BofA variants to localize to the FS (Fig. 3B). As a control, GFPΔ27BofA produced in the *spoIVB165 bofA::erm* double mutant localized discretely to the FS at 3 h PS. Strains producing the N48A and T64A variants showed GFP signal localized to the FS, but signal was also observed in the cytoplasm and possibly at the membrane of the MC, suggesting partial mislocalization. The strain producing the N61A variant appeared to have GFP signal dispersed evenly throughout the MC cytoplasm, suggesting a loss of FS localization. The fusion proteins were intact, suggesting the cytoplasmic signal was not attributable to breakdown (Fig. S6). Inability of the N61A variant to localize to

the FS may explain the loss of SpoIVFB inhibition and the abundant cleavage of Pro-σ^K at 4 h (Fig. 3A, lane 11). Importantly, the similar ability of the N48A and T64A variants to localize to the FS (Fig. 3B) does not account for their differential effects on the level of SpoIVFB and its ability to cleave Pro-σ^K (Fig. 3A). The strain producing GFPΔ27BofA N48A exhibited less SpoIVFB yet more Pro-σ^K cleavage at 4 h (lane 9) than the strain producing GFPΔ27BofA T64A (lane 13), so the N48A substitution more severely impairs the ability of GFPΔ27BofA to inhibit SpoIVFB.

BofA TMS2 Can Occupy the Active Site Region of SpoIVFB. N48 within TMS2 is conserved among BofA orthologs (Fig. S4) and potentially in proximity to the active site of SpoIVFB. The SpoIVFB catalytic core formed by a zinc ion near E44 of the HELGH metalloprotease motif within TMS2 is predicted to be surrounded by five other TMSs in the membrane (Fig. 1A and S7A). The model of the SpoIVFB membrane domain is based on the crystal structure of an archaeal homolog (6). The model is supported by cross-linking studies of catalytically-inactive SpoIVFB E44Q in complex with Pro-σ^K(1-127), whose Proregion is predicted to occupy the SpoIVFB active site region (45, 46, 52). If BofA TMS2 instead occupied the SpoIVFB active site region, it would likely inhibit Pro-σ^K cleavage.

To determine whether BofA TMS2 can occupy the SpoIVFB active site region, we performed disulfide cross-linking experiments that took advantage of the sole Cys residue of BofA, C46, located near N48 in TMS2. We created MBPΔ27BofA because MBP (unlike GFP) contains no Cys residues. As a negative control, we replaced C46 with Ser to obtain Cys-less MBPΔ27BofA C46S. We also created Cys-less SpoIVFA C77L C82L, which cannot form disulfide cross-links. Cys-less SpoIVFA and either MBPΔ27BofA or Cys-less MBPΔ27BofA

were functional when produced from a pET Quartet plasmid, since Pro-σ^K(1-127) cleavage by cytTM-SpoIVFB was inhibited in *E. coli* (Fig. S8). For the disulfide cross-linking experiments, we used Cys-less Pro-σ^K(1-127) C110S and single-Cys variants of cytTM-SpoIVFB created previously (45).

To test whether BofA TMS2 C46 could be cross-linked to a Cys located at the SpoIVFB active site, MBPΔ27BofA C46 and single-Cys E44C cytTM-SpoIVFB were co-produced with Cys-less variants of SpoIVFA and Pro-σ^K(1-127) from a pET Quartet plasmid in *E. coli*. Cells were treated with the oxidant Cu^{2+}(phenanthroline)$_3$ to promote disulfide bond formation. For MBPΔ27BofA C46 (Fig. 4A, lane 2), but not the Cys-less C46S negative control (lane 5), treatment with oxidant caused formation of a species of the expected size for a cross-linked complex with single-Cys E44C cytTM-SpoIVFB, which was detected by immunoblotting with anti-FLAG antibodies. Treatment with the reducing agent DTT greatly diminished the abundance of the apparent complex, consistent with cross-link reversal (lane 3). A species of the expected size for a cross-linked dimer of single-Cys E44C cytTM-SpoIVFB was also observed. Formation of the apparent dimer varies (see below), as reported previously (45). As expected, anti-MBP antibodies detected the presumptive cross-linked complex of MBPΔ27BofA C46 with single-Cys E44C cytTM-SpoIVFB, albeit weakly, and the negative control with E44Q rather than E44C failed to form the complex (Fig. S9, lanes 2 & 5). Since the signal for the complex was stronger with anti-FLAG antibodies (Fig. 4A), we used those antibodies in the cross-linking experiments reported below.

In addition to E44 of SpoIVFB, V70 in a predicted membrane-reentrant loop and P135 in a predicted short loop interrupting TMS4 (Fig. 1A and S7A) were shown to be in proximity to the Proregion of Pro-σ^K(1-127) (45). Therefore, we tested whether MBPΔ27BofA C46 could be

cross-linked to single-Cys V70C or P135C cytTM-SpoIVFB E44Q variants. We included the inactivating E44Q substitution since the V70C and P135C variants (unlike the E44C variant) could cleave Cys-less Pro-σ^K(1-127) (45), even though Cys-less SpoIVFA and either MBPΔ27BofA or Cys-less MBPΔ27BofA were expected to almost completely inhibit cleavage (Fig. S8). MBPΔ27BofA C46 formed a complex with the P135C variant, but not with the V70C variant (Fig. 4B, lanes 2 & 8). As expected, Cys-less MBPΔ27BofA C46S failed to form a complex with either variant (lanes 5 & 11). Full-length BofA C46 also formed a complex of the expected (smaller) size with the E44C and P135C variants, but not with the V70C variant (Fig. S10, lanes 2, 14, & 8). As expected, Cys-less BofA C46S failed to form a complex with any of the variants (lanes 5, 11, & 17). Our cross-linking results show that BofA TMS2 can occupy the active site region of SpoIVFB, placing BofA C46 in proximity to SpoIVFB E44 and P135, but not V70.

Based on our cross-linking results, we modeled BofA TMS2 in the SpoIVFB active site region, and tested predictions of the model using additional disulfide cross-linking experiments (Supplemental Results and Fig. S11). The results confirmed predictions of the initial model and suggested a preferred orientation of BofA TMS2 in the SpoIVFB active site region, which led to a refined model (Fig. S7B).

BofA and SpoIVFA Do Not Prevent Pro-σ^K(1-127) from Interacting with SpoIVFB. Since our cross-linking results show that BofA TMS2 can occupy the SpoIVFB active site region, we tested whether BofA and SpoIVFA prevent Pro-σ^K(1-127) from interacting with SpoIVFB in *E. coli*. Using a catalytically-inactive E44C cytTM-SpoIVFB variant containing the $FLAG_2$ epitope tag but lacking His_6, co-produced Pro-σ^K(1-127), SpoIVFA, and GFPΔ27BofA co-purified with

the cytTM-SpoIVFB variant in pull-down assays with anti-FLAG antibody beads (Fig. 5). All four proteins were seen in the bound sample (lane 4), indicating that GFPΔ27BofA and SpoIVFA did not completely prevent Pro-σ^K(1-127) from interacting with the cytTM-SpoIVFB variant. However, only the cytTM-SpoIVFB variant was detected when the bound sample was diluted tenfold (lane 3) to match the input sample concentration (lane 1), and portions of the other three proteins were observed in the unbound sample (lane 2). The results indicate inefficient co-purification and/or recovery from the beads. A negative control with the cytTM-SpoIVFB variant lacking the $FLAG_2$ epitope tag showed no Pro-σ^K(1-127) in the bound sample, but small amounts of GFPΔ27BofA and SpoIVFA were detected (lane 8), indicative of weak, nonspecific binding to the beads.

We also performed pull-down assays with cobalt resin, which binds to the His_6 tag on Pro-σ^K(1-127), and we performed both types of pull-down assays (i.e., anti-FLAG antibody beads and cobalt resin) when full-length BofA rather than GFPΔ27BofA was co-produced with the other three proteins (Supplemental Results and Fig. S12). Neither BofA nor GFPΔ27BofA when co-produced with SpoIVFA prevented Pro-σ^K(1-127) from interacting with the cytTM-SpoIVFB variant. However, GFPΔ27BofA and SpoIVFA reduced co-purification of full-length Pro-σ^K-His_6 with the cytTM-SpoIVFB variant in both types of pull-down assays (Supplemental Results and Fig. S13), as compared with Pro-σ^K(1-127) (Fig. 5 and S12A), suggesting that the C-terminal half of Pro-σ^K affects complex formation (Supplemental Discussion). As expected, GFPΔ27BofA and SpoIVFA strongly inhibited cytTM-SpoIVFB cleavage of full-length Pro-σ^K-His_6 (Fig. S14), similar to the inhibition of Pro-σ^K(1-127) cleavage we observed (Fig. 1B, lane 4). To further investigate the strong inhibition of cleavage despite the presence of substrate in the pulled-down protein complexes, we next examined the effects of full-length BofA or

MBPΔ27BofA co-produced with SpoIVFA on the interaction of Pro-σ^K(1-127) with cytTM-SpoIVFB using disulfide cross-linking approaches.

Full-length BofA and SpoIVFA Interfere with Cross-Linking between the Proregion of Pro-σ^K(1-127) and the SpoIVFB Active Site Region, and MBPΔ27BofA in Combination with SpoIVFA Is Less Effective at Interfering with Some of the Cross-links. SpoIVFB cleaves Pro-σ^K (43) and Pro-σ^K(1-127) (31) between residues S21 and Y22. In disulfide cross-linking experiments, Cys substitutions for several residues near the cleavage site of otherwise Cys-less Pro-σ^K(1-127) formed a cross-linked complex with single-Cys (E44C, V70C, P135C) cytTM-SpoIVFB variants (45). The complex was most abundant with the E44C and V70C variants, so we compared these interactions in the presence or absence of Cys-less inhibitory proteins.

To examine proximity between single-Cys E44C cytTM-SpoIVFB and the Proregion, we first co-produced single-Cys (F18C, V20C, S21C, K24C) Pro-σ^K(1-127) variants in the absence of inhibitory proteins and measured time-dependent cross-linking. We quantified the cross-linking by measuring the abundance of the complex and dividing that by the total amount of the cytTM-SpoIVFB variant monomer, dimer, and complex. The ratio over time was plotted with a best-fit trend line. Single-Cys E44C cytTM-SpoIVFB formed abundant complex with single-Cys V20C and K24C Pro-σ^K(1-127) variants, and the amount of complex increased over time, but with the F18C and S21C variants much less complex formed, only slightly more than with the Cys-less Pro-σ^K(1-127) negative control (Fig. 6A and S15A). Figure 6B shows a representative immunoblot (60-min oxidant treatment).

Co-production of Cys-less inhibitory proteins greatly reduced complex formation between single-Cys E44C cytTM-SpoIVFB and the V20C and K24C Pro-σ^K(1-127) variants. When Cys-less MBPΔ27BofA and SpoIVFA were co-produced, much less complex formed and its abundance did not increase over time (Fig. 6C and S15B). The decrease in abundance of the complex is most evident comparing representative immunoblots (60-min oxidant treatment) with (Fig. 6D) or without (Fig. 6B) co-produced inhibitory proteins. When Cys-less full-length BofA and SpoIVFA were co-produced, similar decreases in abundance of the complex were observed (Fig. S16). Figure 6E shows a comparison of the cross-linking time courses with and without inhibitory proteins for single-Cys E44C cytTM-SpoIVFB with single-Cys V20C Pro-σ^K(1-127). The effects of Cys-less MBPΔ27BofA and Cys-less full-length BofA were indistinguishable. Similar results were observed with single-Cys K24C Pro-σ^K(1-127) (compare Fig. 6C and S16B). We conclude that MBPΔ27BofA (lacking TMS1) is as effective as full-length BofA at interfering with cross-linking between the Proregion of Pro-σ^K and single-Cys E44C cytTM-SpoIVFB. These results likely explain why BofA TMS1 is dispensable for most of the inhibitory function of BofA (30, 31) (Figs. 1B and 3A). SpoIVFB E44 normally activates a water molecule to hydrolyze the bond between S21 and Y22 of Pro-σ^K. Interfering with this interaction is expected to inhibit cleavage.

We next examined proximity between V70 of SpoIVFB and the Proregion of Pro-σ^K(1-127). V70 is located in a predicted long and potentially flexible membrane-reentrant loop in the SpoIVFB active site region (Fig. 1A and S7A), perhaps explaining why single-Cys V70C cytTM-SpoIVFB E44Q formed abundant cross-linked complex with both the F18C and K24C Pro-σ^K(1-127) variants in the absence of inhibitory proteins (45) (Fig. 6 F and G; Fig. S17 A and B). With co-production of Cys-less variants of MBPΔ27BofA and SpoIVFA, a lower relative

amount of complex was measured, which did not increase over time (Fig. 6 F and G; Fig. S17 C and D), but the impact on complex formation was not as great as when Cys-less variants of full-length BofA and SpoIVFA were co-produced (Fig. 6 F and G; Fig. S17 E and F). Full-length BofA and SpoIVFA also caused four novel species to be observed, including with the Cys-less Pro-σ^K(1-127) negative control (Fig. S17G), perhaps due to cross-linking of the V70C cytTM-SpoIVFB variant to *E. coli* proteins (i.e., BofA may cause the SpoIVFB membrane-reentrant loop to be exposed). In any case, full-length BofA hindered cross-linking more than MBPΔ27BofA (lacking TMS1) (Fig. 6 F and G), suggesting that both TMSs of BofA interfere with the normal interaction between the membrane-reentrant loop of SpoIVFB and the Proregion of Pro-σ^K.

Since full-length BofA also inhibited cleavage of Pro-σ^K(1-127) in *E. coli* (Fig. 1B) and Pro-σ^K in *B. subtilis* (Fig. 3A) slightly more than GFPΔ27BofA (lacking TMS1), we compared time-dependent cross-linking of BofA and MBPΔ27BofA to single-Cys cytTM-SpoIVFB variants. The results suggest that full-length BofA C46 forms slightly more complex with single-Cys E44C cytTM-SpoIVFB and single-Cys P135C cytTM-SpoIVFB E44Q over time, whereas the abundance of complex did not increase over time in the case of MBPΔ27BofA C46 (Fig. S18). Hence, BofA TMS1 may slightly enhance TMS2 occupancy in the active site region of SpoIVFB.

BofA and SpoIVFA Interfere with Cross-Linking between Pro-σ^K(1-127) and the SpoIVFB Interdomain Linker, but Not with Cross-Linking between Pro-σ^K(1-127) and the SpoIVFB CBS Domain. To further examine the effects of the inhibitory proteins on the interaction of Pro-σ^K(1-127) with SpoIVFB, we identified additional residues that formed disulfide cross-linked

complexes. A model of catalytically-inactive SpoIVFB E44Q in complex with Pro-σ^K(1-127) (46) predicts interactions between the C-terminal part of SpoIVFB and parts of Pro-σ^K(1-127). The C-terminal part of SpoIVFB includes a 26-residue interdomain linker and a CBS domain (Fig. 1A and S7A). For both the linker and the CBS domain, we used the model to predict residues of SpoIVFB in proximity to residues of Pro-σ^K(1-127). We tested the predictions by co-producing single-Cys variants of the two proteins and performing disulfide cross-linking experiments. We discovered that a single-Cys Y214C linker variant of cytTM-SpoIVFB E44Q formed abundant complex with single-Cys L41C Pro-σ^K(1-127), and a single-Cys A231C CBS domain variant of cytTM-SpoIVFB E44Q formed complex with single-Cys A97C Pro-σ^K(1-127) (Fig. S19 A and B). We showed that the Cys substitutions do not impair cytTM-SpoIVFB activity or Pro-σ^K(1-127) susceptibility to cleavage (Fig. S19C). Finally, we measured time-dependent cross-linking in the presence or absence of Cys-less inhibitory proteins.

Interestingly, formation of cross-linked complex between the Y214C linker variant of cytTM-SpoIVFB and single-Cys L41C Pro-σ^K(1-127) was hindered more by Cys-less full-length BofA than by Cys-less MBPΔ27BofA, when co-produced with Cys-less SpoIVFA (Fig. 6H and S20A). The pattern is similar to that observed for the V70C membrane-reentrant loop variant of cytTM-SpoIVFB and single-Cys F18C or K24C Pro-σ^K(1-127) (Fig. 6 F and G). The similar pattern suggests that in both cases BofA TMS2 partially interferes with the interaction and BofA TMS1 augments the interference.

Strikingly, co-production of Cys-less inhibitory proteins had little or no effect on formation of cross-linked complex between the A231C CBS domain variant of cytTM-SpoIVFB and single-Cys A97C Pro-σ^K(1-127) (Fig. 6I and S20B). These results suggest that neither full-length BofA nor MBPΔ27BofA, when co-produced with SpoIVFA, prevent Pro-σ^K(1-127) from

interacting with the CBS domain of SpoIVFB in *E. coli*, consistent with our finding that inhibitory proteins did not completely prevent co-purification of SpoIVFB and Pro-σ^K(1-127) (Fig. 5 and S12).

A Model of SpoIVFB in Complex with BofA and Parts of SpoIVFA and Pro-σ^K.

Computational models were generated using a similar protocol as described previously (46), but including additional constraints reflecting experimental cross-linking data reported herein, as well as newly predicted intra- and inter-chain contacts based on co-evolutionary couplings. Two final models were generated: 1) Full-length SpoIVFB modeled as a tetramer, with part of one Pro-σ^K molecule (residues 1-114), referred to as 'fb.sigk'; 2) Full-length SpoIVFB, again modeled as a tetramer, with one molecule each of full-length BofA and parts of Pro-σ^K (residues 38-114) and SpoIVFA (residues 65-111), referred to as 'fb.sigk.bofa.fa'. The omitted residues of Pro-σ^K and SpoIVFA could not be placed with sufficient confidence. The first model is described in Supplemental Methods and Figure S21.

Relevant features of the second model are illustrated in Figure 7 (only one molecule of SpoIVFB is shown). The first side view shows SpoIVFB with BofA TMS2 and the C-terminal part of Pro-σ^K(1-127) (Fig. 7A). The membrane domain of SpoIVFB (green) interacts with BofA TMS2 (cyan) while the interdomain linker and CBS domain of SpoIVFB interact with the modeled portion of Pro-σ^K(1-127) (red). The enlarged view of the SpoIVFB active site region shows BofA TMS2 surrounded by SpoIVFB (TMSs labeled 1-6). The top view of the membrane domain emphasizes proximity between BofA TMS2, SpoIVFB TMSs 2-4, and the zinc ion (magenta) involved in catalysis. The second side view shows SpoIVFB with full-length BofA and the C-terminal part of Pro-σ^K(1-127) (Fig. 7B). Our model predicts that BofA contains 2

TMSs and a membrane-embedded C-terminal region (labeled C near the C-terminus in the enlarged view of the SpoIVFB active site region) that forms two short α-helices connected by a turn. The enlarged and top views show that BofA interacts extensively with SpoIVFB and occupies its active site region, which would sterically hinder access of the Proregion of Pro-σ^K. Figure 7C shows the addition of the modeled portion of SpoIVFA (purple), which is predicted by co-evolutionary couplings to contact the BofA C-terminal region and SpoIVFB TMS4. Hence, the model predicts that SpoIVFA stabilizes the interaction of BofA with SpoIVFB. Since GFPΔ27BofA has the C-terminal region predicted to interact with SpoIVFA, the interaction of GFPΔ27BofA with SpoIVFB is likewise predicted to be stabilized by SpoIVFA, which may explain the dependence of SpoIVFB inhibition on both GFPΔ27BofA and SpoIVFA (Fig. 1C), and why GFPΔ27BofA inhibits substrate cleavage (Fig. 1B and 3A) and MBPΔ27BofA occupies the SpoIVFB active site region (Fig. S18) nearly as well as full-length BofA.

Discussion

Our results provide evidence that BofA occupies the active site region of SpoIVFB. BofA residue C46 near the middle of TMS2 formed disulfide cross-links with SpoIVFB variants containing a single-Cys at (E44C) or near (P135C) its active site. BofA variants containing a single-Cys near the ends of TMS2 formed cross-links with single-Cys SpoIVFB variants that suggest BofA TMS2 adopts a preferred orientation in the SpoIVFB active site region. N48 within BofA TMS2 and both N61 and T64 near its C-terminal end are highly conserved among BofA orthologs. We showed that these residues are important for SpoIVFB inhibition during *B. subtilis* sporulation and upon heterologous expression in *E. coli*. Structural modeling based on partial homology and constraints from cross-linking and co-evolutionary analyses predicts that

439 BofA N48 and T64 interact, and that nearby N61 may also interact to stabilize the BofA
440 structure. SpoIVFA is also important for SpoIVFB inhibition and the model predicts that
441 SpoIVFA bridges the BofA C-terminal region and SpoIVFB to form a membrane-embedded
442 inhibitory complex (Fig. 7C). We found that BofA and SpoIVFA interfere with cross-linking
443 between the Pro-σ^K N-terminal region and the SpoIVFB active site region, supporting a steric
444 hindrance mechanism of SpoIVFB inhibition. BofA TMS1 enhanced interference with some
445 cross-links between Pro-σ^K and SpoIVFB, and slightly enhanced inhibition of SpoIVFB,
446 suggesting that BofA TMS1 enhances steric hindrance of substrate access to the enzyme active
447 site. Our findings have implications for the design of IMMP inhibitors.
448
449 **Conserved Residues May Stabilize BofA in a Membrane-Embedded Inhibitory Complex**
450 **with SpoIVFA that Sterically Hinders Substrate Access to the SpoIVFB Active Site.** BofA,
451 SpoIVFA, and SpoIVFB form a heterotrimeric membrane complex that improves accumulation
452 of each protein likely by inhibiting proteolytic degradation (30). Ala substitutions for N48, N61,
453 and T64 in GFPΔ27BofA reduced its level as well as the levels of SpoIVFA and SpoIVFB, both
454 upon heterologous expression in *E. coli* (Fig. 2) and during *B. subtilis* sporulation (Fig. 3A),
455 suggesting that assembly of the inhibitory complex was impaired. In agreement, the Ala
456 substitutions caused partial or complete mislocalization of GFPΔ27BofA during sporulation (Fig.
457 3B), which normally relies on SpoIVFA (30). Impaired assembly of the inhibitory complex can
458 explain the observed cleavage of Pro-σ^K(1-127) in *E. coli* (Fig. 2) and premature cleavage of
459 Pro-σ^K in sporulating *B. subtilis* (Fig. 3A).
460 Our structural model predicts proximity within BofA between the N48 side chain and a
461 loop that includes N61 and T64. In particular, the T64 side chain is oriented toward the N48 side

462 chain in the model, predicting an interaction. The N61 side chain points away from the N48 and
463 T64 side chains in the model, but the orientation of the N61 side chain is uncertain given the
464 predicted loop structure, so an interaction with the side chains of N48 and/or T64 remains
465 possible. Alternatively, the three conserved residues may contact other residues within BofA,
466 based on co-evolutionary couplings (Supplemental Dataset S4), to stabilize the BofA structure
467 and promote interactions with SpoIVFA and SpoIVFB. For example, disulfide cross-linking
468 supports proximity between BofA L62 and V63 (in the predicted loop that includes N61 and
469 T64) and SpoIVFB M30, which is located in a predicted short loop between TMS1 and TMS2
470 (Fig. S11). Our model satisfies restraints based on this observed cross-linking, as well as many
471 other experimental cross-linking results (45, 46) (Supplemental Dataset S3). The model also
472 predicts numerous interactions between BofA, SpoIVFA, and SpoIVFB that remain to be tested,
473 which will be facilitated by approaches described herein. Of note, the model predicts that BofA
474 C-terminal residues 85 to 87 interact with SpoIVFA and SpoIVFB, and that BofA residues 28 to
475 36 preceding predicted TMS2 interact with SpoIVFA (Fig. 7C), which may explain the effects of
476 deleting or changing those BofA residues, including loss of SpoIVFB inhibition resulting in Pro-
477 σ^K(1-127) cleavage and reduced levels of SpoIVFA and SpoIVFB in *E. coli* (Supplemental
478 Results and Fig. S5). The predicted interactions can be tested further by disulfide cross-linking.
479 BofA and SpoIVFA interfere with cross-linking between the Pro-σ^K N-terminal region
480 and the SpoIVFB active site region, supporting a steric hindrance mechanism of SpoIVFB
481 inhibition. Many latent zymogens likewise use a prosegment or prodomain to sterically hinder
482 substrate access to their active site (53). Many metalloprotease zymogens in addition use a
483 ligand switch mechanism of inhibition and activation. Inhibition involves an amino acid side
484 chain of a residue in the prosegment acting as a metal ligand to prevent catalysis. Activation

485 requires replacement of the side chain metal ligand with a water molecule necessary for substrate
486 peptide bond hydrolysis. BofA residue C46 near the middle of TMS2 is well-positioned in our
487 model to act as a zinc ligand, but C46 is not conserved among BofA orthologs (Fig. S4).
488 Therefore, we favor a simple steric hindrance mechanism of SpoIVFB inhibition. During
489 sporulation, SpoIVFB would be activated when SpoIVB cleaves the C-terminal end of SpoIVFA
490 (35-38) and CtpB cleaves the C-terminal ends of both SpoIVFA and BofA (36, 37, 39) (Fig. S1).
491 These cleavages result in a conformational change in the inhibition complex (36), which we
492 propose allows the Proregion of Pro-σ^K to be positioned in the active site for cleavage. After
493 cleavage, the conformational change may also aid in release of the product, σ^K.
494
495 **BofA TMS1 Appears to Enhance Inhibition of SpoIVFB Slightly by Partially Interfering**
496 **with Its Interaction with Pro-σ^K.** Full-length BofA inhibited cleavage of Pro-σ^K(1-127) in *E.*
497 *coli* (Fig. 1B) and Pro-σ^K in *B. subtilis* (Fig. 3A) slightly more than GFPΔ27BofA. The most
498 likely explanation for the difference, based on our results, is that TMS1 of BofA sterically
499 hinders some interactions between the Pro-σ^K N-terminal region and SpoIVFB more than BofA
500 variants lacking TMS1 (such as GFPΔ27BofA and MBPΔ27BofA). The interactions hindered
501 more by full-length BofA included cross-links between the Pro-σ^K Proregion (F18C and K24C)
502 and the SpoIVFB membrane-reentrant loop (V70C) (Fig. 6F and G), which may bind to the
503 Proregion and present it to the SpoIVFB active site for cleavage (46) based on a study of the
504 homologous membrane-reentrant loop of *E. coli* RseP (54). Our model predicts that both TMSs
505 of BofA, as well as its C-terminal region, occupy the active site region of SpoIVFB (Fig. 7B),
506 which would sterically hinder interactions between the SpoIVFB membrane-reentrant loop and
507 the Pro-σ^K Proregion.

Full-length BofA also hindered cross-links between Pro-σ^K L41C and the SpoIVFB interdomain linker (Y214C) more than MBPΔ27BofA (Fig. 6H). The interdomain linker has been proposed to allow coordination between ATP binding by the CBS domain and Pro-σ^K cleavage by the membrane domain (46). Thus, BofA TMS1 may interfere with coordination between the domains of SpoIVFB by inhibiting movement of the linker, in addition to hindering linker interaction with the Pro-σ^K N-terminal region.

Design of IMMP Inhibitors. Our findings reveal concepts that may inform efforts to design selective inhibitors of IMMPs. BofA TMS2 appears to block the SpoIVFB active site (Fig. 7A), similar to the prosegment of many latent zymogens (53). Like BofA, some prosegments can act in *trans*, an observation that has led to the demonstration of prodomains as selective inhibitors of A Disintegrin And Metalloproteinase (ADAM) family enzymes (55, 56). Selectivity relies on the extensive interaction surface between the prodomain and the enzyme, including features specific to the pair, which can boost efficacy and diminish off-target effects in therapeutic strategies (57). A peptide encompassing residues 48 to 64 of BofA may inhibit SpoIVFB, but our model also predicts extensive interactions between the BofA C-terminal region (residues 65 to 87) and SpoIVFB (Fig. 7B), so a longer BofA peptide, perhaps flexibly linked to SpoIVFA residues 96 to 109, which are also predicted to interact with SpoIVFB (Fig. 7C), may exhibit improved inhibition and selectivity. Since cleavage of Pro-σ^K(1-127) by cytTM-SpoIVFB has been reconstituted *in vitro* (42), it will be possible to test peptides for inhibition. Structure determination of SpoIVFB in complex with an inhibitory peptide, GFPΔ27BofA, or full-length BofA is an important goal to facilitate design of IMMP inhibitors. In particular, it may inform efforts to design inhibitors of SpoIVFB orthologs in *Bacillus* and *Clostridium* species, many of

531 which cause disease or provide benefits, and persist by forming endospores (58). Such efforts
532 could lead to new strategies to control endosporulation.

533 Our findings also suggest that BofA TMS1 interferes with interactions between the Pro-
534 σ^K N-terminal region and SpoIVFB. Therefore, a cyclic peptide inhibitor may prove to be more
535 effective than a linear one. The desirable characteristics of cyclic peptides as therapeutics, and
536 new methods of producing and screening cyclic peptide libraries, make this an attractive
537 possibility (59, 60).

538 The inhibitor design concepts discussed above could apply equally well to IMMPs that
539 normally use one or more PDZ domains to exclude substrate from their active site region. *E. coli*
540 RseP appears to use two PDZ domains to block access of substrate RseA (61-63). Cleavage of
541 the RseA periplasmic domain by DegS (referred to as site-1 cleavage) (64-66) is proposed to
542 allow entry of the RseA TMS into the RseP active site region for site-2 cleavage (67). Recently,
543 batimastat, a hydroxamic acid derivative that mimics the peptide structure of natural substrates,
544 was shown to selectively inhibit RseP *in vivo* (68). Two other peptidomimetic hydroxamic acids,
545 ilomastat and miramastat, exhibited very little RseP inhibition. A lack of selectivity has been a
546 problem in efforts toward using peptidomimetic hydroxamic acids as matrix metalloprotease
547 inhibitors for treatment of cancer, arthritis, and other diseases (57, 69, 70). The hydroxamic acid
548 group of these compounds strongly coordinates the catalytic zinc ion, and the peptidomimetic
549 portions have not provided enough specificity to prevent off-target effects. Even so, the side
550 effects may not preclude using hydroxamic acid-based peptidomimetics to treat bacterial
551 infections topically, and systemically if administered briefly. Perhaps weaker zinc ligands based
552 on amino acid side chains would reduce side effects. A cyclic peptidomimetic with a zinc ligand
553 could presumably block access of the RseA TMS to the RseP active site, or substrate access to

554 the active site of other IMMPs. Other small-molecule matrix metalloprotease inhibitors that
555 have already been developed (69) should be screened for activity against bacteria and fungi with
556 IMMPs known to be involved in pathogenesis (16-19).
557
558 **Materials and Methods**
559 **Plasmids, Primers, and Strains.** Plasmids used in this study are described in Table S1.
560 Primers used in plasmid construction are listed in Table S2. Plasmids were cloned in *E. coli*
561 strain DH5α (71). Relevant parts of plasmids were verified by DNA sequencing with primers
562 listed in Table S3. *B. subtilis* strains used in this study are described in Table S4.
563
564 **Pro-σ^K(1-127) Cleavage in *E. coli*.** Strain BL21(DE3) (Novagen) was used to produce proteins
565 in *E. coli*. Two plasmids with different antibiotic resistance genes were cotransformed (31) or a
566 single plasmid was transformed, with selection on Luria-Bertani (LB) agar supplemented with
567 kanamycin sulfate (50 μg/mL) and/or ampicillin (100 μg/mL). Transformants (4-5 colonies)
568 were grown in LB medium with 50 μg/mL kanamycin sulfate and/or 200 μg/mL ampicillin at
569 37°C with shaking (200 rpm). Typically, overnight culture (200 μL) was transferred to 10 mL of
570 LB medium with antibiotics, cultures were grown at 37°C with shaking (250 rpm) to an optical
571 density of 60-80 Klett units, and isopropyl β-D-thiogalactopyranoside (IPTG) (0.5 mM) was
572 added to induce protein production for 2 h. For transformants with either pET Quintet or full-
573 length Pro-σ^K-His_6, overnight growth was avoided. Transformants were transferred directly to
574 10 mL of LB medium with antibiotic, and cultures were grown and induced as described above.
575 Equivalent amounts of cells (based on optical density in Klett units) were collected (12,000 × *g*

for 1 min) and extracts were prepared (31), then subjected to immunoblot analysis (Supplemental Methods).

BofA Sequence Analysis. Orthologs of *B. subtilis bofA*, which are present in the genomes of most endospore-forming bacteria (20), were collected from the NCBI and Uniprot databases. The protein sequences of BofA orthologs were aligned using the T-Coffee multiple sequence alignment package (72). Residues identical in at least 70% of the sequences were considered conserved.

***B. subtilis* Sporulation and GFPΔBofA Localization.** GFPΔ27BofA or its variants were expressed under control of the *bofA* promoter (P_{bofA}) after ectopic chromosomal integration. Plasmids bearing P_{bofA}-*gfpΔ27bofA* or its variant, bordered by regions of homology to *B. subtilis amyE*, were transformed into strain ZR264. Transformants with a gene replacement at *amyE* were selected on LB agar with spectinomycin sulfate (100 μg/mL) and identified by loss of amylase activity (73). Sporulation was induced by growing cells in the absence of antibiotics followed by the resuspension of cells in SM medium (73). At indicated times PS, samples (50 μL) were centrifuged (12,000 × *g* for 1 min), supernatants were removed, and cell pellets were stored at -80°C. Whole-cell extracts were prepared as described for *E. coli* (31), except samples were incubated at 50°C for 3 min instead of boiling for 3 min (46), and proteins were subjected to immunoblot analysis (Supplemental Methods).

To image GFPΔ27BofA localization, samples collected at 3 h PS were examined by fluorescence microscopy using an Olympus FluoView FV-1000 filter-based confocal microscope. GFPΔ27BofA (ex/em ~488/507 nm) was excited using a 458 nM argon laser and

599 fluorescence was captured using a BA465-495 nm band pass filter. The lipophilic dye FM 4-64
600 (1 μg/mL) (AAT Bioquest) was used to stain membranes. FM 4-64 (ex/em ~515/640 nm) was
601 excited using a 515 nm argon laser and fluorescence was captured using a BA560IF band pass
602 filter (74).
603
604 **Disulfide Cross-Linking.** A method described previously (75) was used with slight
605 modifications (45). Briefly, as described above for Pro-σ^K(1-127) cleavage, *E. coli* BL21(DE3)
606 was transformed with a plasmid, grown in LB (10 mL), induced with IPTG, and equivalent
607 amounts of cells were collected. Cells were subjected to disulfide cross-linking, then lysed and
608 proteins were precipitated by addition of trichloroacetic acid (5%), and proteins were subjected
609 to immunoblot analysis (Supplemental Methods).
610
611 **Co-Immunoprecipitation (FLAG$_2$ Pull-Down Assays).** *E. coli* BL21(DE3) was transformed
612 with a plasmid, grown in LB (1 L), and induced with IPTG as described above. The culture was
613 split, cells were harvested, and cell pellets were stored at -80°C. Cell lysates were prepared as
614 described (52), except that each cell pellet was resuspended in 20 mL of lysis buffer containing
615 50 mM Tris-HCl pH 7.1 rather than PBS. Cell lysates were centrifuged (15,000 × *g* for 15 min
616 at 4 °C) to sediment cell debris and protein inclusion bodies. The supernatant was treated with
617 1% *n*-dodecyl-β-D-maltoside (DDM) (Anatrace) for 1 h at 4 °C to solubilize membrane proteins,
618 then centrifuged at 150,000 × *g* for 1 h at 4 °C. The supernatant was designated the input sample
619 and 1 mL was mixed with 50 uL anti-DYKDDDDK magnetic agarose (Pierce) that had been
620 equilibrated with buffer (50 mM Tris-HCl pH 7.1, 0.1% DDM, 5 mM 2-mercaptoethanol, 10%
621 glycerol) and the mixture was rotated for 1 h at 25°C. The magnetic agarose was removed with a

622 DynaMag-2 magnet (Invitrogen) and the supernatant was saved (unbound sample). The
623 magnetic agarose was washed three times by gently vortexing with 500 μL wash buffer (50 mM
624 Tris-HCl pH 7.1, 150 mM NaCl, 10% glycerol, 0.1% DDM), then washed once with 500 μL
625 water. The magnetic agarose was mixed with 50 μL of 2× sample buffer (50 mM Tris·HCl pH
626 6.8, 4% SDS, 20% glycerol, 200 mM DTT 0.03% bromophenol blue) and boiled for 3 min
627 (bound sample). A portion of the bound sample was diluted tenfold (1/10 bound sample) with
628 1× sample buffer to match the concentration of the input sample. Samples were subjected to
629 immunoblot analysis (Supplemental Methods).
630
631 **Colbalt Affinity Purification (His_6 Pull-Down Assays).** Input sample (15 mL) prepared as
632 described above was mixed with imidazole (5 mM) and 0.5 mL of Talon superflow metal affinity
633 resin (Clontech) that had been equilibrated with buffer (as above for magnetic agarose). The
634 mixture was rotated for 1 h at 4°C. The cobalt resin was sedimented by centrifugation at 708 × *g*
635 for 2 min at 4 °C and the supernatant was saved (unbound sample). The resin was washed three
636 times with 5 mL wash buffer (as above plus 5 mM imidazole), each time rotating the mixture for
637 10 min at 4 °C and sedimenting resin as above. The resin was mixed with 0.5 mL 2× sample
638 buffer and boiled for 3 min (bound sample). A portion of the bound sample was diluted
639 fifteenfold (1/15 bound sample) with 1× sample buffer to match the concentration of the input
640 sample. Samples were subjected to immunoblot analysis (Supplemental Methods).
641
642 **Modeling of Complexes Containing SpoIVFB, BofA, and Parts of SpoIVFA and Pro-σ^K.**
643 The modeling proceeded through stages where initial monomeric models were assembled step-
644 by-step into multimeric complexes guided primarily by the restraints from cross-linking

experiments and predicted contacts from co-evolutionary coupling analysis. More specifically, a SpoIVFB monomer was first assembled from the membrane and CBS domains. Two monomers were combined into a dimer and the dimer was assembled into a plausible tetramer. Part of one molecule of Pro-σ^K (residues 1-114) was subsequently added, which resulted in 'fb.sigk'. The 'fb.sigk.bofa.fa' model was developed by starting from 'fb.sigk', truncating the Pro-σ^K N-terminus (residues 1-37), and subsequently adding first BofA and finally SpoIVFA (residues 65-111). See Supplemental Methods for additional description of the modeling.

ACKNOWLEDGMENTS. We thank Daniel Parrell for assistance with fluorescence microscopy, Jon Kaguni for helpful comments on the manuscript, and David Rudner, Simon Cutting, Ruanbao Zhou, and Yang Zhang for plasmids. This research was supported by National Institutes of Health Grants R01 GM43585 (to L.K.) and R35 GM126948 (to M.F.), and by Michigan State University AgBioResearch.

References

1. Brown MS, Ye J, Rawson RB, Goldstein JL (2000) Regulated intramembrane proteolysis: a control mechanism conserved from bacteria to humans. *Cell* 100:391-398.
2. Urban S (2013) Mechanisms and cellular functions of intramembrane proteases. *Biochim. Biophys. Acta - Biomembr.* 1828:2797-2800.
3. Manolaridis I, *et al.* (2013) Mechanism of farnesylated CAAX protein processing by the intramembrane protease Rce1. *Nature* 504:301-305.
4. Hu J, Xue Y, Lee S, Ha Y (2011) The crystal structure of GXGD membrane protease FlaK. *Nature* 475:528-531.

5. Li X, *et al.* (2013) Structure of a presenilin family intramembrane aspartate protease. *Nature* 493:56-61.
6. Feng L, *et al.* (2007) Structure of a site-2 protease family intramembrane metalloprotease. *Science* 318:1608-1612.
7. Wang Y, Zhang Y, Ha Y (2006) Crystal structure of a rhomboid family intramembrane protease. *Nature* 444:179-183.
8. Wu Z, *et al.* (2006) Structural analysis of a rhomboid family intramembrane protease reveals a gating mechanism for substrate entry. *Nat. Struct. Mol. Biol.* 13:1084-1091.
9. Cho S, Dickey SW, Urban S (2016) Crystal structures and inhibition kinetics reveal a two-stage catalytic mechanism with drug design implications for rhomboid proteolysis. *Mol. Cell* 61:329-340.
10. Zoll S, *et al.* (2014) Substrate binding and specificity of rhomboid intramembrane protease revealed by substrate-peptide complex structures. *Embo J.* 33:2408-2421.
11. Yang G, *et al.* (2019) Structural basis of Notch recognition by human γ-secretase. *Nature* 565:192-197.
12. Zhou R, *et al.* (2019) Recognition of the amyloid precursor protein by human γ-secretase. *Science* 363:eaaw0930.
13. Rawson RB (2013) The site-2 protease. *Biochim. Biophys. Acta - Biomembr.* 1828:2801-2807.
14. Ye J (2013) Roles of regulated intramembrane proteolysis in virus infection and antiviral immunity. *Biochim. Biophys. Acta - Biomembr.* 1828:2926-2932.
15. Adam Z (2013) Emerging roles for diverse intramembrane proteases in plant biology. *Biochim. Biophys. Acta - Biomembr.* 1828:2933-2936.

16. Chang YC, Bien CM, Lee H, Espenshade PJ, Kwon-Chung KJ (2007) Sre1p, a regulator of oxygen sensing and sterol homeostasis, is required for virulence in *Cryptococcus neoformans*. *Mol. Microbiol.* 64:614-629.

17. Urban S (2009) Making the cut: central roles of intramembrane proteolysis in pathogenic microorganisms. *Nat. Rev. Microbiol.* 7:411-423.

18. Kroos L, Akiyama Y (2013) Biochemical and structural insights into intramembrane metalloprotease mechanisms. *Biochim. Biophys. Acta - Biomembr.* 1828:2873-2885.

19. Schneider JS, Glickman MS (2013) Function of site-2 proteases in bacteria and bacterial pathogens. *Biochim. Biophys. Acta - Biomembr.* 1828:2808-2814.

20. Galperin MY, *et al.* (2012) Genomic determinants of sporulation in *Bacilli* and *Clostridia*: towards the minimal set of sporulation-specific genes. *Environ. Microbiol.* 14:2870-2890.

21. McKenney PT, Driks A, Eichenberger P (2013) The *Bacillus subtilis* endospore: assembly and functions of the multilayered coat. *Nat. Rev. Microbiol.* 11:33-44.

22. Al-Hinai MA, Jones SW, Papoutsakis ET (2015) The *Clostridium* sporulation programs: diversity and preservation of endospore differentiation. *Microbiol. Mol. Biol. Rev.* 79:19-37.

23. Checinska A, Paszczynski A, Burbank M (2015) *Bacillus* and other spore-forming genera: variations in responses and mechanisms for survival. *Annu. Rev. Food Sci. Technol.* 6:351-369.

24. Cutting S, *et al.* (1990) A forespore checkpoint for mother-cell gene expression during development in *Bacillus subtilis*. *Cell* 62:239-250.

25. Cutting S, Roels S, Losick R (1991) Sporulation operon *spoIVF* and the characterization of mutations that uncouple mother-cell from forespore gene expression in *Bacillus subtilis*. *J. Mol. Biol.* 221:1237-1256.

714 26. Ricca E, Cutting S, Losick R (1992) Characterization of *bofA*, a gene involved in
715 intercompartmental regulation of pro-σ^K processing during sporulation in *Bacillus subtilis*. *J.*
716 *Bacteriol.* 174:3177-3184.
717 27. Tan IS, Ramamurthi KS (2014) Spore formation in *Bacillus subtilis*. *Environ. Microbiol.*
718 *Rep.* 6:212-225.
719 28. Resnekov O, Alper S, Losick R (1996) Subcellular localization of proteins governing the
720 proteolytic activation of a developmental transcription factor in *Bacillus subtilis*. *Genes Cells*
721 1:529-542.
722 29. Rudner DZ, Pan Q, Losick RM (2002) Evidence that subcellular localization of a bacterial
723 membrane protein is achieved by diffusion and capture. *Proc Natl Acad Sci U S A* 99:8701-
724 8706.
725 30. Rudner DZ, Losick R (2002) A sporulation membrane protein tethers the pro-σ^K processing
726 enzyme to its inhibitor and dictates its subcellular localization. *Genes Dev.* 16:1007-1018.
727 31. Zhou R, Kroos L (2004) BofA protein inhibits intramembrane proteolysis of pro-σ^K in an
728 intercompartmental signaling pathway during *Bacillus subtilis* sporulation. *Proc. Natl. Acad.*
729 *Sci. USA* 101:6385-6390.
730 32. Kroos L, Yu YT, Mills D, Ferguson-Miller S (2002) Forespore signaling is necessary for
731 pro-σ^K processing during *Bacillus subtilis* sporulation despite the loss of SpoIVFA upon
732 translational arrest. *J. Bacteriol.* 184:5393-5401.
733 33. Cutting S, Driks A, Schmidt R, Kunkel B, Losick R (1991) Forespore-specific transcription
734 of a gene in the signal transduction pathway that governs pro-σ^K processing in *Bacillus*
735 *subtilis*. *Genes Dev.* 5:456-466.

736 34. Pan Q, Losick R, Rudner DZ (2003) A second PDZ-containing serine protease contributes to
737 activation of the sporulation transcription factor σ^K in *Bacillus subtilis*. *J. Bacteriol.*
738 185:6051-6056.
739 35. Dong TC, Cutting SM (2003) SpoIVB-mediated cleavage of SpoIVFA could provide the
740 intercellular signal to activate processing of Pro-σ^K in *Bacillus subtilis*. *Mol. Microbiol.*
741 49:1425-1434.
742 36. Campo N, Rudner DZ (2006) A branched pathway governing the activation of a
743 developmental transcription factor by regulated intramembrane proteolysis. *Mol. Cell* 23:25-
744 35.
745 37. Campo N, Rudner DZ (2007) SpoIVB and CtpB are both forespore signals in the activation
746 of the sporulation transcription factor σ^K in *Bacillus subtilis*. *J. Bacteriol.* 189:6021-6027.
747 38. Mastny M, *et al.* (2013) CtpB assembles a gated protease tunnel regulating cell-cell signaling
748 during spore formation in *Bacillus subtilis*. *Cell* 155:647-658.
749 39. Zhou R, Kroos L (2005) Serine proteases from two cell types target different components of
750 a complex that governs regulated intramembrane proteolysis of pro-σ^K during *Bacillus*
751 *subtilis* development. *Mol. Microbiol.* 58:835-846.
752 40. Rudner D, Fawcett P, Losick R (1999) A family of membrane-embedded metalloproteases
753 involved in regulated proteolysis of membrane-associated transcription factors. *Proc. Natl.*
754 *Acad. Sci. USA* 96:14765-14770.
755 41. Yu Y-TN, Kroos L (2000) Evidence that SpoIVFB is a novel type of membrane
756 metalloprotease governing intercompartmental communication during *Bacillus subtilis*
757 sporulation. *J. Bacteriol.* 182:3305-3309.

42. Zhou R, Cusumano C, Sui D, Garavito RM, Kroos L (2009) Intramembrane proteolytic cleavage of a membrane-tethered transcription factor by a metalloprotease depends on ATP. *Proc. Natl. Acad. Sci. USA* 106:16174-16179.

43. Kroos L, Kunkel B, Losick R (1989) Switch protein alters specificity of RNA polymerase containing a compartment-specific sigma factor. *Science* 243:526-529.

44. Eichenberger P, *et al.* (2004) The program of gene transcription for a single differentiating cell type during sporulation in *Bacillus subtilis*. *PLoS Biol.* 2:e328.

45. Zhang Y, Luethy PM, Zhou R, Kroos L (2013) Residues in conserved loops of intramembrane metalloprotease SpoIVFB interact with residues near the cleavage site in Pro-σ^K. *J. Bacteriol.* 195:4936-4946.

46. Halder S, Parrell D, Whitten D, Feig M, Kroos L (2017) Interaction of intramembrane metalloprotease SpoIVFB with substrate Pro-σ^K. *Proc. Natl. Acad. Sci. USA* 114:E10677-E10686.

47. Saribas AS, Gruenke L, Waskell L (2001) Overexpression and purification of the membrane-bound cytochrome P450 2B4. *Protein Expr. Purif.* 21:303-309.

48. Prince H, Zhou R, Kroos L (2005) Substrate requirements for regulated intramembrane proteolysis of *Bacillus subtilis* pro-σ^K. *J. Bacteriol.* 187:961-971.

49. Ramirez-Guadiana FH, *et al.* (2018) Evidence that regulation of intramembrane proteolysis is mediated by substrate gating during sporulation in *Bacillus subtilis*. *PLoS Genet.* 14:e1007753.

50. de Hoon MJ, Eichenberger P, Vitkup D (2010) Hierarchical evolution of the bacterial sporulation network. *Curr. Biol.* 20:R735-R745.

780 51. Varcamonti M, Marasco R, De Felice M, Sacco M (1997) Membrane topology analysis of
781 the *Bacillus subtilis* BofA protein involved in pro-σ^K processing. *Microbiol.* 143:1053-1058.
782 52. Zhang Y, *et al.* (2016) Complex formed between intramembrane metalloprotease SpoIVFB
783 and its substrate, Pro-σ^K. *J. Biol. Chem.* 291:10347-10362.
784 53. Arolas JL, Goulas T, Cuppari A, Gomis-Ruth FX (2018) Multiple architectures and
785 mechanisms of latency in metallopeptidase zymogens. *Chem. Rev.* 118:5581-5597.
786 54. Akiyama K, *et al.* (2015) Roles of the membrane-reentrant β-hairpin-like loop of RseP
787 protease in selective substrate cleavage. *eLife* 4:e08928
788 55. Moss ML, *et al.* (2007) The ADAM10 prodomain is a specific inhibitor of ADAM10
789 proteolytic activity and inhibits cellular shedding events. *J. Biol. Chem.* 282:35712-35721.
790 56. Wong E, *et al.* (2016) Harnessing the natural inhibitory domain to control TNFα Converting
791 Enzyme (TACE) activity *in vivo*. *Sci. Rep.* 6:35598.
792 57. Gomis-Ruth FX (2017) Third time lucky? Getting a grip on matrix metalloproteinases. *J.*
793 *Biol. Chem.* 292:17975-17976.
794 58. Driks A, Eichenberger P eds (2016) *The bacterial spore: from molecules to systems* (ASM
795 Press, Washington, DC), p 397.
796 59. Zorzi A, Deyle K, Heinis C (2017) Cyclic peptide therapeutics: past, present and future.
797 *Curr. Opin. Chem. Biol.* 38:24-29.
798 60. Sohrabi C, Foster A, Tavassoli A (2020) Methods for generating and screening libraries of
799 genetically encoded cyclic peptides in drug discovery. *Nat. Rev. Chem.* 4:90-101.
800 61. Grigorova IL, *et al.* (2004) Fine-tuning of the *Escherichia coli* σ^E envelope stress response
801 relies on multiple mechanisms to inhibit signal-independent proteolysis of the
802 transmembrane anti-sigma factor, RseA. *Genes Dev.* 18:2686-2697.

803 62. Inaba K, *et al.* (2008) A pair of circularly permutated PDZ domains control RseP, the S2P
804 family intramembrane protease of *Escherichia coli*. *J. Biol. Chem.* 283:35042-35052.
805 63. Kanehara K, Ito K, Akiyama Y (2003) YaeL proteolysis of RseA is controlled by the PDZ
806 domain of YaeL and a Gln-rich region of RseA. *EMBO J.* 22:6389-6398.
807 64. Ades SE, Connolly LE, Alba BM, Gross CA (1999) The *Escherichia coli* σ^E-dependent
808 extracytoplasmic stress response is controlled by the regulated proteolysis of an anti-sigma
809 factor. *Genes Dev.* 13:2449-2461.
810 65. Alba BM, Leeds JA, Onufryk C, Lu CZ, Gross CA (2002) DegS and YaeL participate
811 sequentially in the cleavage of RseA to activate the σ^E-dependent extracytoplasmic stress
812 response. *Genes Dev.* 16:2156-2168.
813 66. Kanehara K, Ito K, Akiyama Y (2002) YaeL (EcfE) activates the σ^E pathway of stress
814 response through a site-2 cleavage of anti-σ^E, RseA. *Genes Dev.* 16:2147-2155.
815 67. Hizukuri Y, *et al.* (2014) A structure-based model of substrate discrimination by a
816 noncanonical PDZ tandem in the intramembrane-cleaving protease RseP. *Structure* 22:326-
817 336.
818 68. Konovalova A, *et al.* (2018) Inhibitor of intramembrane protease RseP blocks the σ^E
819 response causing lethal accumulation of unfolded outer membrane proteins. *Proc. Natl.*
820 *Acad. Sci. USA* 115:E6614-E6621.
821 69. Jacobsen JA, Major Jourden JL, Miller MT, Cohen SM (2010) To bind zinc or not to bind
822 zinc: an examination of innovative approaches to improved metalloproteinase inhibition.
823 *Biochim. Biophys. Acta* 1803:72-94.
824 70. Fields GB (2015) New strategies for targeting matrix metalloproteinases. *Matrix Biol.* 44-
825 46:239-246.

826 71. Hanahan D (1983) Studies on transformation of *Escherichia coli* with plasmids. *J. Mol. Biol.*
827 166:557-580.
828 72. Notredame C, Higgins DG, Heringa J (2000) T-Coffee: A novel method for fast and accurate
829 multiple sequence alignment. *J. Mol. Biol.* 302:205-217.
830 73. Harwood CR, Cutting SM (1990) *Molecular Biological Methods for Bacillus* (John Wiley &
831 Sons, Chichester, England) p 581.
832 74. Parrell D, Kroos L (2020) Channels modestly impact compartment-specific ATP levels
833 during *Bacillus subtilis* sporulation and a rise in the mother cell ATP level is not necessary
834 for Pro-σ^K cleavage. *Mol. Microbiol.* 114:563-581.
835 75. Koide K, Ito K, Akiyama Y (2008) Substrate recognition and binding by RseP, an
836 *Escherichia coli* intramembrane protease. *J. Biol. Chem.* 283:9562-9570.
837
838

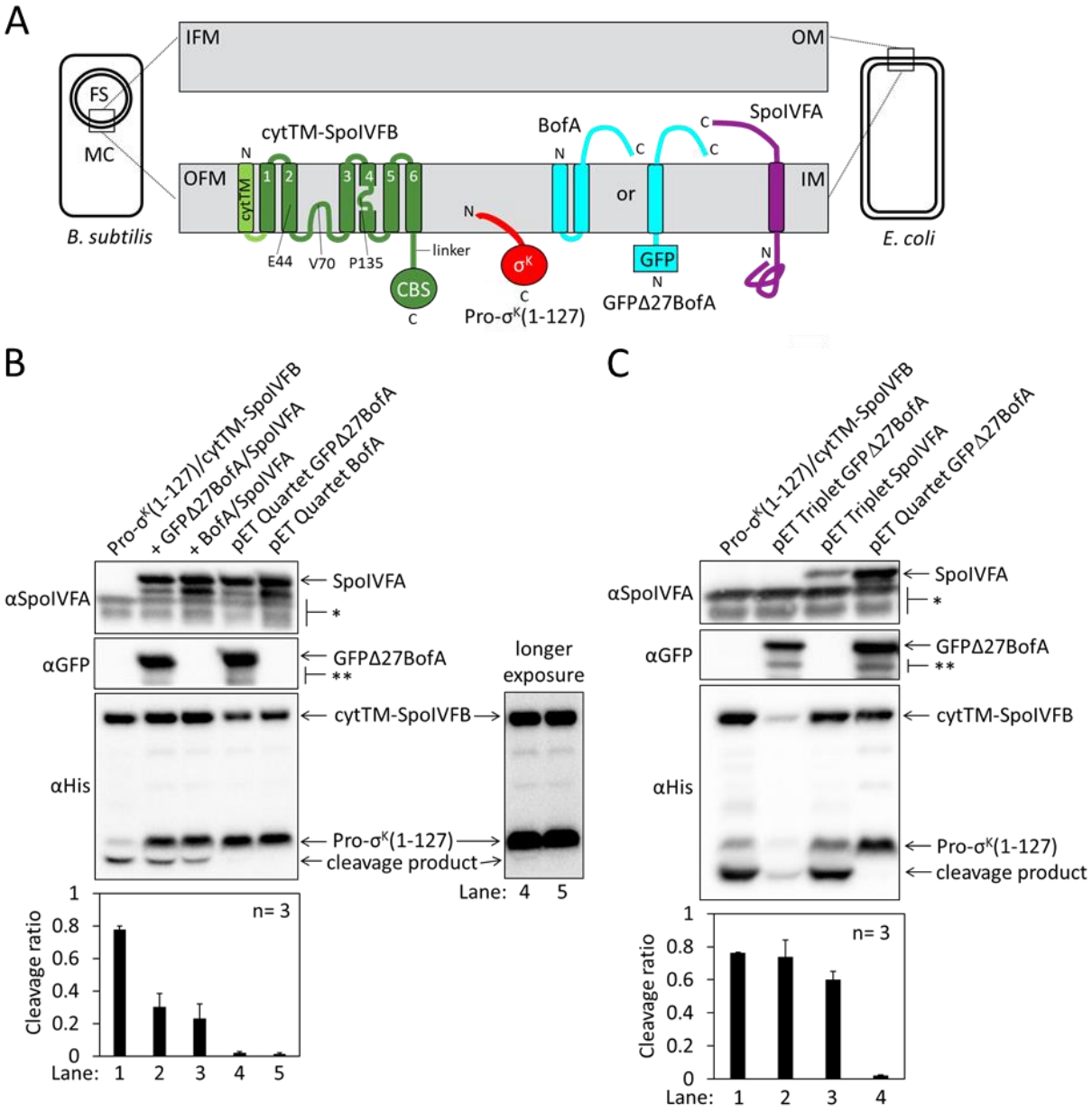

Fig. 1. Inhibition of Pro-σ^K cleavage. (*A*) Diagram of SpoIVFB inhibition during *B. subtilis* endosporulation and upon heterologous expression in *E. coli*. During endosporulation (*Left*), SpoIVFB and its inhibitory proteins BofA and SpoIVFA are produced in the mother cell (MC) and localize to the outer forespore (FS) membrane (OFM). Pro-σ^K is also produced in the MC and associates with membranes. When these proteins are synthesized in *E. coli* (*Right*), they localize to the inner membrane (IM). The expanded view of the membranes (*Center*) shows a SpoIVFB variant with an extra N-terminal transmembrane segment (cytTM), and highlights several residues (E44, V70, P135) at or near the active site in the membrane domain, which is connected to the CBS domain by an interdomain linker. When produced in *E. coli*, cytTM-SpoIVFB cleaves Pro-σ^K(1-127), removing its N-terminal Proregion. Co-production of SpoIVFA and either full-length BofA or GFPΔ27BofA (lacking predicted TMS1) inhibits Pro-σ^K(1-127) cleavage. (*B*) Cleavage assays comparing inhibition by SpoIVFA and either

GFPΔ27BofA or full-length BofA in *E. coli*. Pro-σ^K(1-127) and cytTM-SpoIVFB were produced alone (lane 1, pYZ2) or in combination with GFPΔ27BofA and SpoIVFA (lane 2, pYZ46) or full-length BofA and SpoIVFA (lane 3, pSO212). Alternatively, "pET Quartet" plasmids were used to produce Pro-σ^K(1-127), cytTM-SpoIVFB, SpoIVFA, and either GFPΔ27BofA (lane 4, pSO40) or full-length BofA (lane 5, pSO213). Samples collected after 2 h of IPTG induction were subjected to immunoblot analysis with SpoIVFA (*Top*), GFP (*Middle*), or penta-His antibodies (*Bottom*, 2 and 30 s exposures). The single star (*) indicates cross-reacting proteins below SpoIVFA and the double star (**) indicates breakdown species of GFPΔ27BofA. A breakdown species below SpoIVFA (not indicated) is observed in some experiments. The graph shows quantification of the cleavage ratio (cleavage product/[Pro-σ^K(1-127) + cleavage product]) for three biological replicates. Error bars, 1 standard deviation. (*C*) Cleavage assays comparing inhibition by either GFPΔ27BofA or SpoIVFA. pET Triplet plasmids were used to produce Pro-σ^K(1-127), cytTM-SpoIVFB, and either GFPΔ27BofA (lane 2, pSO64) or SpoIVFA (lane 3, pSO65). Samples were subjected to immunoblot analysis and quantification as in *B*.

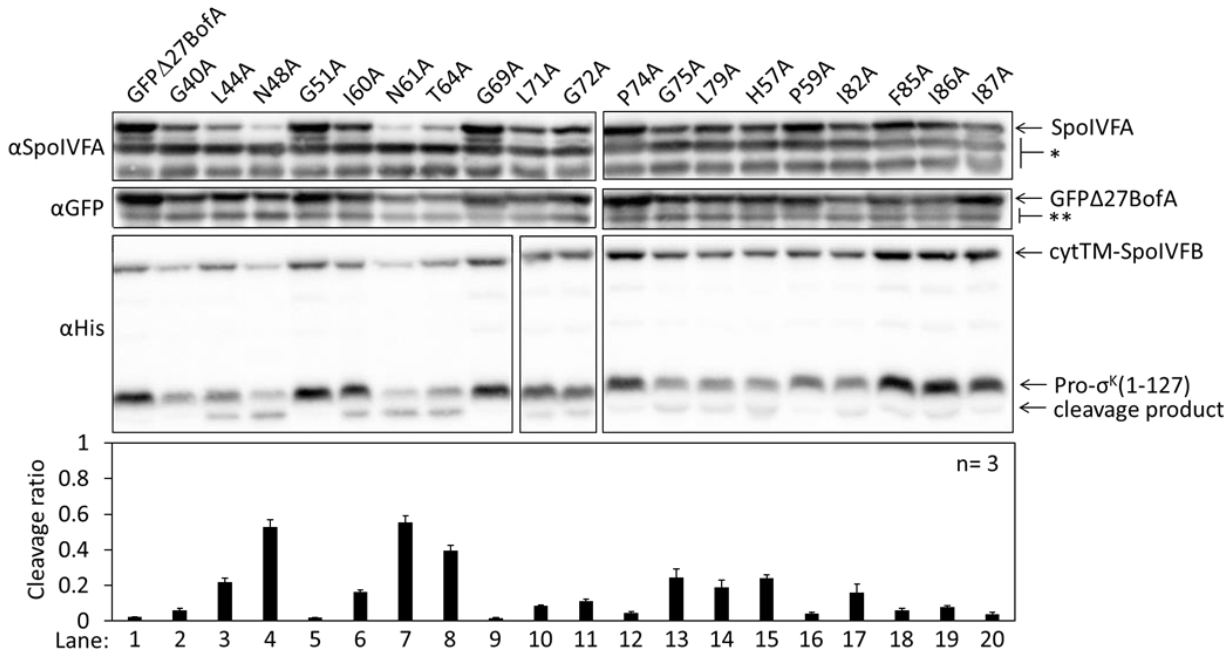

Fig. 2. Effects of alanine substitutions in GFPΔ27BofA on inhibition of Pro-σ^K(1-127) cleavage in *E. coli*. pET Quartet plasmids were used to produce Pro-σ^K(1-127), cytTM-SpoIVFB, SpoIVFA, and GFPΔ27BofA (lane 1, pSO40) or Ala-substituted GFPΔ27BofA (lanes 2-20, pSO44-pSO58 and pSO60-pSO63). Samples collected after 2 h of IPTG induction were subjected to immunoblot analysis with SpoIVFA, GFP, and penta-His antibodies. Single (*) and double (**) stars are explained in the Figure 1B legend, as is the graph.

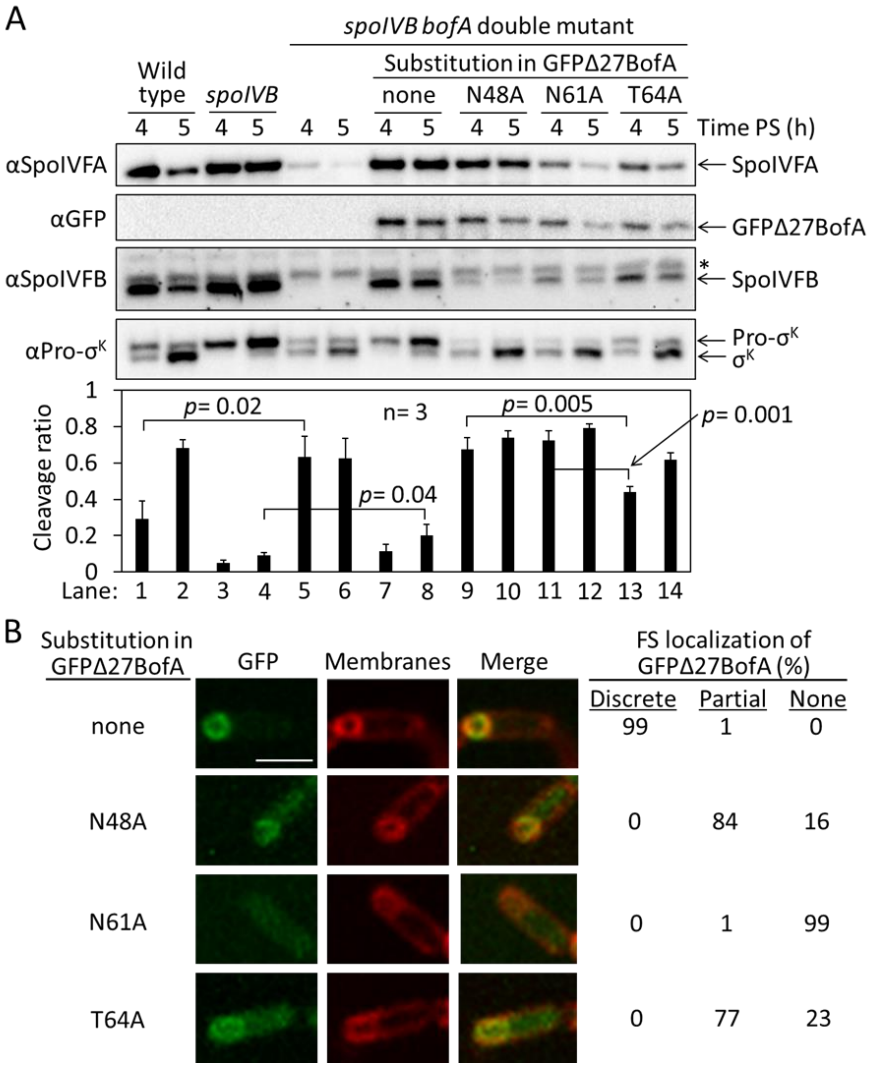

Fig. 3. Effects of alanine substitutions in GFPΔ27BofA during *B. subtilis* sporulation. (*A*) Effects of GFPΔ27BofA variants (N48A, N61A, T64A) on Pro-σ^K cleavage. Wild-type strain PY79, a *spoIVB165* null mutant, a *spoIVB165 bofA::erm* double mutant, and the double mutant with P_{bofA}-*gfpΔ27bofA* integrated ectopically at *amyE* to express GFPΔ27BofA with no substitution (none) or the indicated Ala substitution, were starved to induce sporulation. Samples collected at 4 and 5 h poststarvation (PS) were subjected to immunoblot analysis with antibodies against SpoIVFA, GFP, SpoIVFB, and Pro-σ^K. The graph shows quantification of the cleavage ratio [cleavage product/(Pro-σ^K + cleavage product)] for three biological replicates. Error bars, 1 standard deviation. Student's two-tailed *t* tests were performed to compare certain cleavage ratios (*p* values). (*B*) Localization of GFPΔ27BofA and the three variants. Samples collected at 3 h PS were treated with FM 4-64 to stain membranes. Confocal microscopy images of fluorescence from GFPΔ27BofA, membranes, and merged images are shown for representative sporangia with discrete (no substitution in GFPΔ27BofA, designated "none"), partial (N48A and T64A), or no forespore (FS) localization (N61A). Scale bar, 1 μm. The percentage of sporangia (44-93 counted; non-sporulating cells were not counted) with each localization pattern is shown.

894

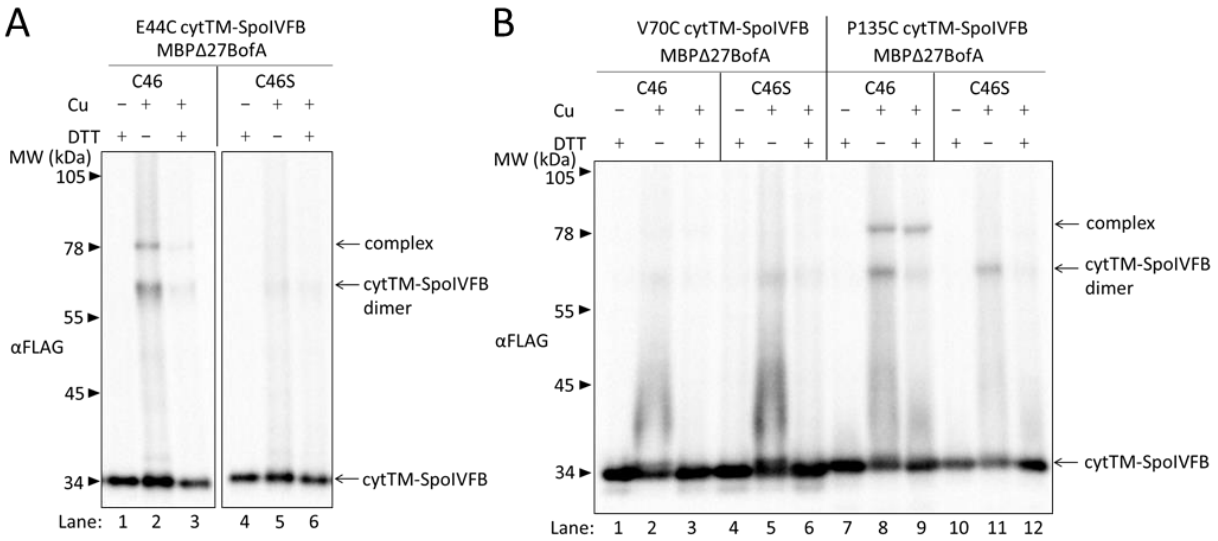

Fig. 4. MBPΔ27BofA TMS2 is near the cytTM-SpoIVFB active site. (*A*) Disulfide cross-linking of single-Cys E44C cytTM-SpoIVFB to MBPΔ27BofA C46. pET Quartet plasmids were used to produce single-Cys E44C cytTM-SpoIVFB in combination with MBPΔ27BofA C46 (pSO91) or Cys-less MBPΔ27BofA C46S as a negative control (pSO110), and Cys-less variants of SpoIVFA and Pro-σ^K(1-127) in *E. coli*. Samples collected after 2 h of IPTG induction were treated with Cu^{2+}(phenanthroline)$_3$ (Cu +) for 60 min or with 2-phenanthroline (Cu –) as a control. Samples were treated with TCA to precipitate proteins and resuspended in sample buffer with DTT (+) or without (–) and subjected to immunoblot analysis with FLAG antibodies to visualize cytTM-SpoIVFB monomer, dimer, and complex with MBPΔ27BofA. (*B*) Disulfide cross-linking of single-Cys V70C or P135C cytTM-SpoIVFB E44Q variants to MBPΔ27BofA C46. pET Quartet plasmids were used to produce single-Cys V70C or P135C cytTM-SpoIVFB E44Q variants in combination with MBPΔ27BofA (pSO92, pSO93) or Cys-less MBPΔ27BofA C46S as a negative control (pSO111, pSO112), and Cys-less variants of SpoIVFA and Pro-σ^K(1-127) in *E. coli*. Samples collected after 2 h of IPTG induction were treated and subjected to immunoblot analysis as in *A*. A representative result from at least two biological replicates is shown in *A* and *B*.

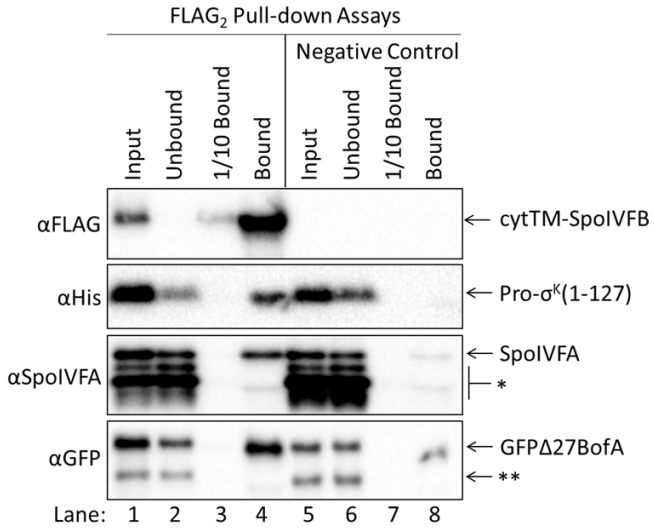

Fig. 5. GFPΔ27BofA and SpoIVFA do not prevent Pro-σ^K(1-127) from co-purifying with SpoIVFB. pET Quartet plasmids were used to produce a catalytically-inactive E44C cytTM-SpoIVFB variant containing $FLAG_2$ but lacking His_6 (pSO73), or a variant also lacking $FLAG_2$ as a negative control (pSO149), in combination with Pro-σ^K(1-127), GFPΔ27BofA, and SpoIVFA in *E. coli*. Samples collected after 2 h of IPTG induction were subjected to co-immunoprecipitation with anti-FLAG antibody beads. Input, unbound, 1/10 bound (diluted to match input), and (undiluted) bound samples were subjected to immunoblot analysis with FLAG, penta-His, SpoIVFA, and GFP antibodies. The single star (*) indicates cross-reacting proteins below SpoIVFA and the double star (**) indicates a cross-reacting protein or breakdown species of GFPΔ27BofA that fail to co-purify. A representative result from two biological replicates is shown.

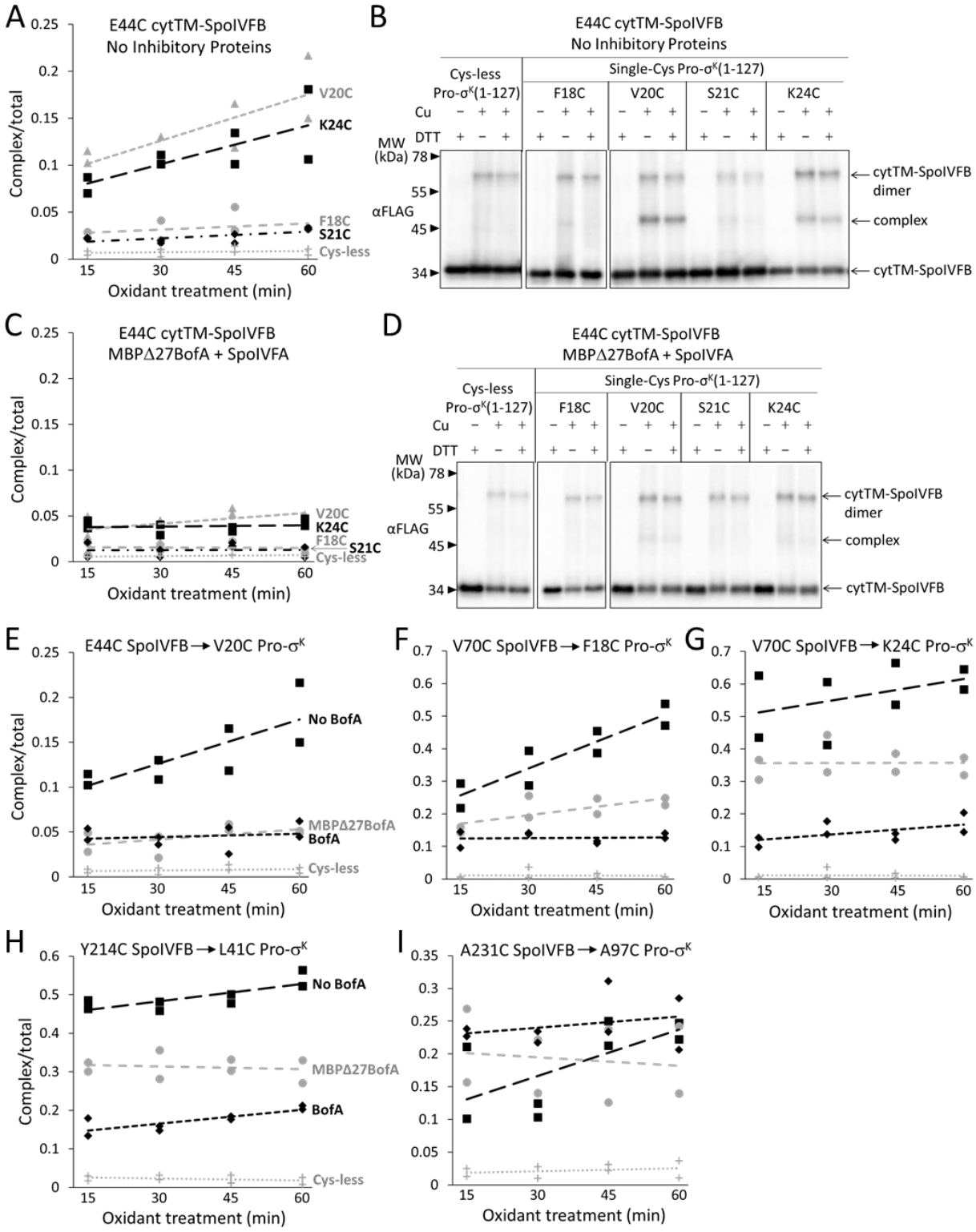

Fig. 6. Effects of inhibitory proteins on cross-linking between cytTM-SpoIVFB and Pro-σ^K(1-127). (*A*) Quantification of disulfide cross-linking between single-Cys E44C cytTM-SpoIVFB and single-Cys Pro-σ^K(1-127) variants in the absence of inhibitory proteins. pET Duet plasmids were used to produce single-Cys E44C cytTM-SpoIVFB in combination with single-Cys F18C

(pSO167), V20C (pSO169), S21C (pSO170), or K24C (pSO128) Pro-σ^K(1-127), or with Cys-less Pro-σ^K(1-127) (pSO79) as a negative control, in *E. coli*. Samples collected after 2 h of IPTG induction were treated with Cu^{2+}(phenanthroline)$_3$ (oxidant; Cu + in *B*) for 15, 30, 45, or 60 min or with 2-phenanthroline (Cu – in *B*) as a control. Samples were treated with TCA to precipitate proteins and resuspended in sample buffer with DTT (+ in *B*) or without (– in *B*) and subjected to immunoblot analysis with FLAG antibodies to visualize the cytTM-SpoIVFB monomer, dimer, and complex with Pro-σ^K(1-127) (Fig. S15A). Abundance of the complex was divided by the total amount of cytTM-SpoIVFB monomer, dimer, and complex. The ratio over time was plotted (n=2) with a best-fit trend line. (*B*) Representative immunoblots of 60-min samples from the experiment described in *A*. (*C*) Quantification of cross-linking between single-Cys E44C cytTM-SpoIVFB and single-Cys Pro-σ^K(1-127) variants in the presence of Cys-less variants of MBPΔ27BofA and SpoIVFA. pET Quartet plasmids were used to produce single-Cys E44C cytTM-SpoIVFB in combination with single-Cys F18C (pSO163), V20C (pSO165), S21C (pSO166), or K24C (pSO131) Pro-σ^K(1-127), or with Cys-less Pro-σ^K(1-127) (pSO110) as a negative control, and Cys-less variants of MBPΔ27BofA and SpoIVFA in *E. coli*. Samples collected after 2 h of IPTG induction were treated and subjected to immunoblot analysis as in *A* (Fig. S15B). (*D*) Representative immunoblots of 60-min samples from the experiment described in *C*. (*E*) Quantification of cross-linking between single-Cys E44C cytTM-SpoIVFB and single-Cys V20C Pro-σ^K(1-127) in the absence or presence of inhibitory proteins. Data from *A* (No BofA), *C* (MBPΔ27BofA), and Figure S16A (full-length BofA) are plotted along with Cys-less Pro-σ^K(1-127) as a negative control. (*F* and *G*) Quantification of cross-linking between single-Cys V70C cytTM-SpoIVFB E44Q and single-Cys F18C or K24C Pro-σ^K(1-127) variants in the absence or presence of inhibitory proteins. Data from Figure S17 are plotted using symbols and lines as in *E*. (*H* and *I*) Quantification of cross-linking between single-Cys Y214C or A231C cytTM-SpoIVFB E44Q and single-Cys L41C or A97C Pro-σ^K(1-127) in the absence or presence of inhibitory proteins. Data from Figure S20 are plotted using symbols and lines as in *E*.

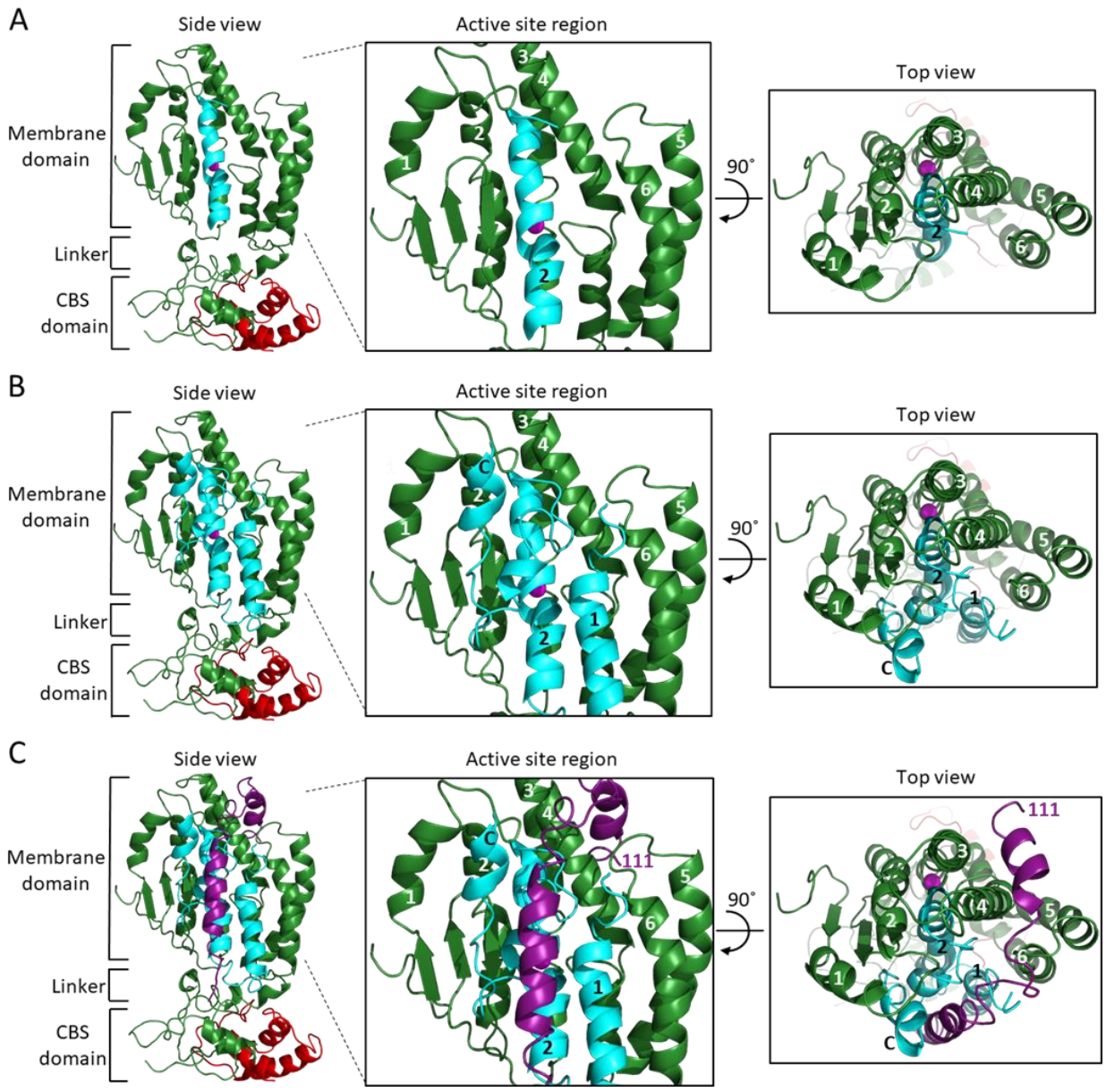

Fig. 7. Model of SpoIVFB monomer with BofA and parts of SpoIVFA and Pro-σ^K. (*A*) Model of SpoIVFB, BofA TMS2, and the C-terminal part of Pro-σ^K(1-127). At *Left*, a side view of the complex, showing the six TMSs of the SpoIVFB membrane domain with the active site zinc ion (magenta), the interdomain linker, and the CBS domain (green), BofA TMS2 (cyan), and Pro-σ^K(38-114) (red). In the enlarged view of the active site region (*Center*), TMSs 1– 6 of SpoIVFB and TMS2 of BofA are numbered. At *Right*, a top view is shown. (*B*) Model of SpoIVFB with full-length BofA and Pro-σ^K(38-114). Predicted TMSs 1 and 2 of BofA are numbered and its C-terminal region is labeled "C" near the C-terminus in the views shown in the *Center* and at *Right*. (*C*) Model of SpoIVFB with full-length BofA, SpoIVFA(65-111) (purple, residue 111 is numbered), and Pro-σ^K(38-114).